Electronic state spectroscopy of methyl formate probed by high resolution VUV photoabsorption, He(I) photoelectron spectroscopy and ab initio calculations

Journal Item

Electronic state spectroscopy of methyl formate probed by high resolution VUV photoabsorption, He(I) photoelectron spectroscopy and *ab initio* calculations

Y. Nunes,[a] G. Martins,[a] N. J. Mason,[b] D. Duflot,[c] S. V. Hoffmann,[d] J. Delwiche,[e] M.-J. Hubin-Franskin[e] and P. Limão-Vieira*[ab]

Received 29th March 2010, Accepted 21st July 2010
DOI: 10.1039/c0cp00051e

The first *ab initio* calculations of the vertical excitation energies and oscillator strengths are presented for the neutral electronic transitions of methyl formate, $C_2H_4O_2$. The highest resolution VUV photoabsorption spectrum of the molecule yet reported is presented over the wavelength range 115 to 310 nm (10.8 to 4.0 eV) revealing several new spectral features. Valence and Rydberg transitions and their associated vibronic series, observed in the photoabsorption spectrum, have been assigned in accordance with new theoretical results. The calculations have been carried out to determine the excitation energies of the lowest energy ionic states of methyl formate and are compared with a newly recorded He(I) photoelectron spectrum (10.4 to 17.0 eV). New vibrational structure is observed in the first photoelectron band. The photoabsorption cross-sections have been used to calculate the photolysis lifetime of methyl formate in the upper stratosphere (20–50 km).

1. Introduction

Methyl formate has been widely used as an industrial solvent, a blowing agent for foam isolation, and as a replacement for the CFCs, HCFCs or HFCs, having zero ozone depletion and global warming potentials.[1] It can also be used as an insecticide and to manufacture, formamide, dimethyl formamide and formic acid.[1]

Methyl formate is also known as formic acid methyl ester and is an isomeric form of acetic acid. In a recent publication we reported the electronic state spectroscopy of acetic acid using high resolution vacuum ultraviolet photoabsorption, electron impact, He(I) photoelectron spectroscopy and *ab initio* calculations, where a detailed analysis of the vibrational progressions and several Rydberg series were proposed for the first time.[2]

A Zero Kinetic Energy (ZEKE) photoelectron spectrum of methyl formate has been reported by Waterstradt *et al.*[3] and the absolute optical oscillator strength for the (π^*(C=O) ← n_O) transition in methyl formate has been calculated by Rocha *et al.*;[4] these authors also measured the UV photoabsorption cross-section of this absorption band (4.8–6.1 eV) which was found to be in good agreement with Vesine and Mellouki.[5]

In this paper we present high resolution VUV photoabsorption spectra with absolute cross-sections together with the first theoretical calculations of the vertical excitation energies and oscillator strengths of the electronic transitions of methyl formate. As far as we are aware, these are the first high resolution studies reported for this molecule.

We have also experimentally measured and analysed the He(I) photoelectron spectrum, particularly in order to clarify Rydberg assignments in the VUV spectrum also with the first ionic band resolved for the first time. Absolute photoabsorption cross-sections are needed in modelling studies of the Earth atmosphere, radiation chemistry and physics of esters.

2. Experimental procedure

2.1 VUV photoabsorption

The high-resolution VUV photoabsorption spectrum of methyl formate was measured using the UV1 beam line of the ASTRID synchrotron facility at the University of Aarhus, Denmark. The experimental apparatus has been described in detail elsewhere.[6] Briefly, synchrotron radiation passes through a static gas sample and a photomultiplier is used to measure the transmitted light intensity. The incident wavelength is selected using a toroidal dispersion grating with 2000 lines per mm providing a resolution of 0.075 nm, corresponding to 3 meV at the midpoint of the energy range studied. For wavelengths below 200 nm (energies above 6.20 eV), helium was flushed through the small gap between the photomultiplier and the exit window of the gas cell to prevent any absorption by air contributing to the spectrum. The sample pressure is measured using a capacitance manometer (Baratron). To ensure that the data are free of any saturation effects the

[a] *Laboratório de Colisões Atómicas e Moleculares, CEFITEC, Departamento de Física, FCT, Universidade Nova de Lisboa, 2829-516 Caparica, Portugal. E-mail: plimaovieira@fct.unl.pt; Fax: +351 21 294 85 49; Tel: +351 21 294 78 59*
[b] *Centre of Earth, Planetary, Space and Astronomy Research, Department of Physics and Astronomy, The Open University, Walton Hall, Milton Keynes, MK7 6AA, UK*
[c] *Laboratoire de Physique des Lasers, Atomes et Molécules (PhLAM), UMR CNRS 8523, Université Lille1 Science s et Technologies, F-59655 Villeneuve d'Ascq Cedex, France*
[d] *Institute for Storage Ring Facilities, Aarhus University, Ny Munkegade, DK-8000, Århus C, Denmark*
[e] *Laboratoire de Spectroscopie d'Électrons diffusés, Université de Liège, Institut de Chimie-Bât. B6c, B-4000 Liège, Belgium*

absorption cross-sections were measured over the pressure range 0.04–0.75 Torr, with typical attenuations of less than 10%. The synchrotron beam ring current was monitored throughout the collection of each spectrum and background scans were recorded with the cell evacuated. Absolute photoabsorption cross-sections are then obtained using the Beer–Lambert attenuation law: $I_t = I_0 \exp(-n\sigma x)$, where I_t is the radiation intensity transmitted through the gas sample, I_0 is that through the evacuated cell, n the molecular number density of the sample gas, σ the absolute photoabsorption cross-section, and x the absorption path length (25 cm). The accuracy of the cross-section is estimated to be ±5%. Only when absorption by the sample is very weak ($I_0 \approx I_t$), does the error increase as a percentage of the measured cross-section.

2.2 Photoelectron spectroscopy

The He(I) (21.22 eV) photoelectron spectrum of methyl formate, $C_2H_4O_2$, was recorded at room temperature at the Université de Liège, Belgium. The experimental set-up has been described elsewhere.[7] Briefly, the spectrometer consists of a 180° cylindrical electrostatic analyser with a mean radius of 5 cm. The analyser was used in constant energy pass mode and was fitted with a continuous dynode electron multiplier. The incident photons were produced by a dc He discharge in a two-stage differentially pumped lamp.

The energy scale was calibrated using two peaks in xenon ($^2P_{3/2}$ = 12.130 eV and $^2P_{1/2}$ = 13.436 eV)[8] mixed in the methyl formate gas stream. These spectra were corrected for the transmission function of the apparatus. The photoelectron spectrum presented in this paper is the sum of 56 individual spectra. This procedure allows us to obtain a good signal-to-noise ratio while keeping the pressure in the spectrometer at a very low level ($<1.5 \times 10^{-6}$ Torr). The resolution of the present photoelectron spectrum is measured from the FWHM of the Xe^+ peaks to be 30 meV, in the presence of methyl formate. The accuracy of the energy scale is estimated to be ±2 meV.

2.3 Methyl formate samples

The liquid samples used in the VUV and PES measurements were purchased from Fluka with a quoted purity of 99.8%. The samples were degassed by repeated freeze–pump–thaw cycles prior to use.

3. Computational methods

Ab initio calculations were performed to determine the geometries as well as the excitation energies of the neutral states (Table 1) and the ionic states (Table 2). In a first step, the ground state geometry was optimised at the MP2 level using the Dunning's aug-cc-pVTZ basis set.[9] Harmonic vibrational frequencies were also computed analytically at MP2 level.

For the calculation of UV spectra, it is well known that obtaining accurate vertical excitation energies and oscillator strengths remains a difficult task even for small organic molecules such as methyl formate (see for example ref. 10 for a recent review). The computational cost of TDDFT methods is low but they are known to have problems when dealing with Rydberg or charge transfer states.[11] Multireference methods such as CASPT2[12] or CASSCF/MRCI techniques become prohibitive when a large number of Rydberg orbitals have to be included in the active space. On the other hand, Coupled Cluster methods have recently proven to give reliable results and appear to be a good compromise between computational cost and accuracy.[13] The electronic spectrum of methyl formate was thus computed at the EOM-CCSD level.[14] To this end, a set of diffuse functions (6s, 6p, 4d), taken from Kaufmann *et al.*[15] and localized on the central oxygen atom, were added to the original basis set for a better description of the Rydberg states (aug-cc-pVTZ + R basis set). The corresponding oscillator strengths were calculated in the length gauge (in atomic units):

$$f_L = \tfrac{2}{3}\Delta E |\langle \Psi_{gs}|\boldsymbol{r}|\Psi_{exc}\rangle|^2$$

The lowest vertical ionisation energies of methyl formate were also obtained at the RCCSD[16] and RCCSD(T) levels.[17] All these calculations were performed using the MOLPRO programme.[18] In order to obtain higher ionisation energies, additional Partial Third Order (P3) propagation calculations[19,20] were performed using the Gaussian03 package.[21] Concerning the geometry of ionised methyl formate, it is logical to employ the same level of computation as for the neutral molecule, *i.e.*, MP2. However, it is well known[22] that in the case of open shell systems, there are several possible MP2 methods. The method we have chosen in the present work is the ZAPT technique,[23] implemented within the GAMESS-US program.[24,25] Consequently, harmonic frequencies for the ions were obtained numerically rather than analytically. Finally, in order to interpret the vibrational structure we used the ezSpectrum program.[26,27] These calculations take into account the Duschinsky rotations between the ground and the ion vibration.[28]

4. Brief summary of the structures and properties of methyl formate, $C_2H_4O_2$

Methyl formate, $C_2H_4O_2$, has C_s symmetry in its electronic ground state. The symmetry species available are thus A′ and A″. The calculated electron configuration of the $\tilde{X}^1A'$ ground state is as follows: (a) core orbitals $(1a')^2$ $(2a')^2$ $(3a')^2$ $(4a')^2$; (b) valence orbitals $(5a')^2$ $(6a')^2$ $(7a')^2$ $(8a')^2$ $(9a')^2$ $(10a')^2$ $(1a'')^2$ $(11a')^2$ $(2a'')^2$ $(12a')^2$ $(3a'')^2$ $(13a')^2$. The highest occupied molecular orbital (HOMO, 13a′) in the neutral ground state is localized essentially on the oxygen in-plane lone pair (n_O). The second highest occupied orbital (3a″) corresponds to the bonding π(C═O) with a slightly antibonding character on the central oxygen out-of-plane p lone pair. The lowest unoccupied molecular orbital (LUMO) is mainly of π* antibonding character localized on the (C═O) group, (π*(C═O)).

The MP2 calculated geometry is shown in Fig. 1(a), with the interatomic distances. The present values are in good agreement with the best "semi-experimental" equilibrium structure,[29] obtained by combining rotational spectroscopy and *ab initio* methods. Our geometry is also consistent with the results of Cui *et al.*[30] obtained at the CASSCF/MRCI/cc-pVDZ level and those of Senent *et al.*[31] (MP4(SDTQ)/cc-pVQZ level).

Table 1 Calculated vertical excitation energies (EOM-CCSD/aug-cc-pVTZ + R//MP2/aug-cc-pVTZ) (eV) and oscillator strengths compared with the present experimental vertical energies and VUV absorption cross-sections of methyl formate, $C_2H_4O_2$

State	E/eV	f_L	$\langle r^2 \rangle^a$	Main character	Exp./eV	Cross-section/Mb
$\tilde{X}^1A'$	—	—	53			
$^1A''$	5.892	0.00131	53	13a′ → LUMO	5.87(9)	0.2
$^1A'$	7.946	0.00437	84	13a′ → 3sσ/σ*(CH)	7.48(2)	9.5
$^1A'$	8.206	0.15297	66	3a″ → LUMO	8.372	25.3
$^1A''$	8.429	0.00915	88	3a″ → 3sσ/σ*(CH_3)	8.18(9)	22.3
$^1A'$	8.587	0.04793	103	13a′ → 3pσ/σ*(CH)	8.492	19.8
$^1A''$	8.812	0.00335	113	13a′ → 3pπ		
$^1A'$	8.940	0.01651	119	13a′ → 3pσ/σ*(CH)	8.682	23.6
$^1A''$	9.045	0.02197	102	3a″ → 3pσ/σ*(CH_3)	9.123	20.7
$^1A''$	9.184	0.00017	55	12a′ → LUMO		
$^1A'$	9.204	0.05295	119	13a′ → 3dσ	9.252	20.6
$^1A'$	9.296	0.03219	111	3a″ → 3dπ	9.848	19.8
$^1A''$	9.364	0.00260	105	3a″ → 3pσ/σ*(CH)	9.43(6)	15.3
$^1A''$	9.462	0.00833	117	3a″ → 3dσ		
$^1A'$	9.651	0.00226	176	13a′ → 3dσ′		
$^1A'$	9.657	0.00287	202	13a′ → 3dσ″		
$^1A''$	9.658	0.00010	177	13a′ → 3dπ		
$^1A''$	9.735	0.00043	188	13a′ → 3dπ′		
$^1A'$	9.784	0.00943	261	13a′ → 4sσ	9.322	15.5
$^1A''$	9.990	0.00090	364	13a′ → 4pπ		
$^1A'$	9.939	0.01041	335	13a′ → 4pσ	9.679	15.1
$^1A'$	10.014	0.00017	312	13a′ → 4pσ′	9.770	16.8
$^1A'$	10.099	0.00434	178	3a″ → 3dπ′ + 12a′ → 3sσ		
$^1A''$	10.108	0.00050	162	3a″ → 3dσ′		
$^1A'$	10.134	0.00839	410	13a′ → 4dσ	9.943	23.1
$^1A'$	10.153	0.02205	167	3a″ → 3dπ′ + 12a′ → 3sσ		
$^1A''$	10.184	0.00169	188	3a″ → 3dσ″		
$^1A'$	10.204	0.00192	179	3a″ → 3dπ′		
$^1A''$	10.282	0.00069	262	3a″ → 4pσ	10.306	27.1
$^1A'$	10.300	0.00276	598	13a′ → 4dσ′		
$^1A''$	10.310	0.00004	562	13a′ → 4dπ		
$^1A'$	10.310	0.00119	566	13a′ → 4dσ″		
$^1A''$	10.331	0.00015	589	13a′ → 4dπ′		
$^1A'$	10.359	0.00445	733	13a′ → 5sσ	9.963	24.2
$^1A'$	10.429	0.00273	900	13a′ → 5pσ	10.125	25.6
$^1A''$	10.425	0.00533	316	3a″ → 4pσ′	10.454	28.2
$^1A''$	10.452	0.00042	964	13a′ → 5pπ		
$^1A'$	10.475	0.00160	957	13a′ → 5pσ′	10.171	25.3
$^1A'$	10.501	0.01290	357	3a″ → 4pπ		
$^1A'$	10.529	0.00585	967	13a′ → 5dσ	10.26(4)	24.8
$^1A''$	10.544	0.00015	357	3a″ → 4dσ		
$^1A''$	10.569	0.00166	371	3a″ → 4dσ′		
$^1A'$	10.598	0.01642	291	12a′ → 3pσ/σ*(CH)		
$^1A'$	10.616	0.00324	1419	13a′ → 5dσ′		
$^1A'$	10.654	0.00009	1133	13a′ → 5dσ″		
$^1A''$	10.660	<0.00001	794	13a′ → 5dπ		
$^1A'$	10.679	0.00221	1465	13a′ → 6sσ	10.272	25.3
$^1A'$	10.695	0.00238	1136	13a′ → 6pσ	10.358	27.0
$^1A'$	10.712	0.00297	1225	13a′ → 6pσ′	10.384	25.7
$^1A'$	10.754	0.00501	1020	13a′ → 6dσ	10.43(2)	26.4

[a] Mean value of r^2 (electronic radial spatial extents). The last decimal of the energy value is given in brackets for these less-resolved features.

After ZPE corrections the MP2 energy separation between the two equilibrium conformations *cis* and *trans* is calculated to be 0.23 eV (22.2 kJ mol^{-1}). This difference is identical to the value calculated by Senent *et al.*[31] but slightly higher than the recent value of 0.14 eV (13.8 kJ mol^{-1}) obtained by Cui *et al.*[30] Only the *cis* isomer (Fig. 1(a)) is thus present at room temperature and therefore the *trans* isomer may not contribute to the VUV and PE spectra discussed in Sections 5 and 6, respectively.

Previous experimental studies reported an adiabatic ionisation energy (IE) of methyl formate of 10.835 eV.[3] The present photoelectron measurement of the adiabatic IE of methyl formate is 10.812 eV (Section 6). In the present analysis of the VUV spectra, adiabatic ionisation energies have been used to calculate quantum defects in order to identify the Rydberg character of several excited states (Section 5.2).

5. Electronic state spectroscopy results and discussion

The present VUV spectrum of methyl formate is shown in Fig. 2. The major absorption bands can be classified mainly as members of Rydberg series and valence transitions with ($\pi_{CO}^* \leftarrow n_O$, 13a′), ($\sigma^* \leftarrow n_O$, 13a′) and ($\pi_{CO}^* \leftarrow \pi_{CO}$, 3a″) character. The same character has also been observed for acetic acid.[2] In the low-energy part of the present range, the

Table 2 Calculated and experimental He(I) photoelectron energies (MOLPRO/MP2/aug-cc-pVTZ geometry) of methyl formate (eV)

	This work (calculated)					Exp.		
Configuration	P3[a]	RMP2[a]	ZAPT[b]	RCCSD[a]	RCCSD(T)[a]	This work	Ref. 3	Ref. 40
$\tilde{X}^2A'$ ($13a'^{-1}$)	11.320	11.494	11.555/11.142	11.045	11.126	10.997/10.812[c]	10.835[c]	10.85[d]
$\tilde{A}^2A''$ ($3a''^{-1}$)	11.862	12.656	12.779/12.170	11.787	11.742	11.536	11.554[c]	11.6
$^2A'$ ($12a'^{-1}$)	13.380	—	—	—	—	13.173	13.145[c]	13.2
$^2A''$ ($2a''^{-1}$)	14.344	—	—	—	—	14.177	13.964[c]	14.2
$^2A'$ ($11a'^{-1}$)	15.160	—	—	—	—	15.000	14.791[c]	15.0
$^2A''$ ($1a''^{-1}$)	16.847	—	—	—	—	16.490	16.403[c]	16.5
$^2A'$ ($10a'^{-1}$)	16.884	—	—	—	—	—	17.453[c]	17.5
$^2A'$ ($9a'^{-1}$)	18.353	—	—	—	—	—	18.398[c]	18.5
$^2A'$ ($8a'^{-1}$)	20.520	—	—	—	—		19.746[c]	19.9

[a] Vertical values. [b] GAMESS-US results: vertical/adiabatic. [c] Adiabatic values. [d] Adiabatic value from ref. 41.

calculations reported in Table 1 indicate that the electronic transitions have mixed valence–Rydberg character. Accordingly, the low-energy VUV bands show characteristics associated with both types of transitions.

5.1 Valence state spectroscopy of methyl formate

According to the calculations summarised in Table 1, the absorption bands centred at 5.87(9), 7.48(2) and 8.372 eV have been assigned to (π^*(C═O) ← n_O, 13a′), (3sσ/σ*(CH) ← n_O, 13a′) and (π^*(C═O) ← π(C═O), 3a″) transitions, respectively (Fig. 2–5). Pure Rydberg transitions with high oscillator strengths in this energy range are discussed in Section 5.2. The first band, with a maximum absolute cross-sections of 0.2 Mb, has been identified as the transition from the oxygen in-plane lone pair to the first π antibonding MO (π^*(C═O) ← n_O, 13a′), $1^1A''$ ← $\tilde{X}^1A'$). Considering the broad nature of the structures in this band, the present maximum at 5.87(9) eV is in reasonable agreement with Rocha *et al.*'s result (5.766 eV).[4] Our calculated oscillator strength (1.31×10^{-3}) is close to the value of 1.08×10^{-3} obtained by Rocha *et al.*[4] However, it should be noticed that these authors showed that vibrational corrections are needed to obtain a theoretical value close to the experimental value of 1.78×10^{-3}. Centred at 7.48(2) eV with a maximum cross-section of 9.5 Mb, the second band is assigned mainly to the (3sσ/σ*(CH) ← n_O, 13a′, $2^1A'$ ← $1^1A'$) transition. Although the calculations indicate a mixed valence/Rydberg character (3sσ), the rather high calculated intensity is primarily due to the important valence σ*(CH) character of the MO. With a local maximum cross-section of 25.3 Mb at 8.372 eV, the third band is assigned to a (π^*(C═O) ← π(C═O), 3a″), ($3^1A'$ ← $1^1A'$) transition.

The structure between 5.0 and 6.5 eV (Fig. 3 and Table 3) is mainly assigned to excitation to the π^*(C═O) anti-bonding orbital from the HOMO (n_O, 13a′). Accordingly, the associated vibronic series is proposed to be due to the C–O stretching (ν_8),[32] although the broad nature of the features suggests that further modes and combinations may also contribute to the observed structure. In particular, the normal mode configuration may lead to Fermi resonances, notably around the feature at 5.42(1) eV, due to the ν_4 C═O stretching. The feature at 5.22(2) eV is tentatively assigned as the origin of the band.

Further overlap of vibronic structures associated with both valence and Rydberg transitions is proposed to account for the features above 7.8 eV (Fig. 4 and 5 and Table 3). However, the complexity of the structure makes it difficult to assign transitions unambiguously. Indeed the present calculations (Table 1) predict a number of low-intensity transitions (Rydberg) which cannot be identified unambiguously in the VUV spectrum.

The vibronic structure beginning at 7.48(2) eV (Table 3) is proposed to be due to a mixed Rydberg/valence character (Fig. 4 and Table 1) combined with only one quanta of C═O stretching (ν_4) mode. The electronic transition associated with the vibronic progression originating at 7.822 eV has been identified as $2^1A'$ ← $1^1A'$ due to the (π^*(C═O) ← π(C═O), 3a″) valence transition. The spacing between features in the vibrational excitation is similar to that observed in the lowest ionic state (Section 6). The C═O stretching mode (ν_4) (associated with π^*(C═O) ← π(C═O)) is also coupled with the CH_3 symmetric deformation (ν_6) mode (Fig. 4).

5.2 Pure Rydberg transitions

The VUV spectrum above 7.4 eV consists of a few structures superimposed on a diffuse absorption feature extending to the two lowest ionisation energies (IE). The proposed Rydberg structures are labelled in Fig. 2 and 5 and are presented in Tables 4 and 5. The peak positions, E_n, have been tested using the Rydberg formula: $E_n = E_i - R/(n - \delta)^2$, where E_i is the ionisation energy (IE_1) with an adiabatic value of 10.812 eV and IE_2 the vertical value has a value of 11.536 eV, n is the principal quantum number of the Rydberg orbital of energy E_n, R is the Rydberg constant (13.610 eV), and δ the quantum defect resulting from the penetration of the Rydberg orbital into the core. Quantum defects in the range 0.9–1.0, ~0.5, and 0.02–0.16 are expected for ns, np, and nd transitions, respectively.[33]

The feature at 7.48(2) eV (Table 1) is tentatively assigned to the Rydberg transition (3sσ* ← n_O, 13a′) with a quantum defect $\delta = 0.98$ (Table 4). The $n = 4$ member may be accompanied by vibronic structure, as previously reported for the valence transition (π^*(C═O) ← π(C═O), 3a″, $3^1A'$ ← $1^1A'$), which is proposed to be mainly due to excitation of the ν_4 mode (Fig. 5 and Table 4). The higher members of this Rydberg series are proposed to extend to $n = 9$.

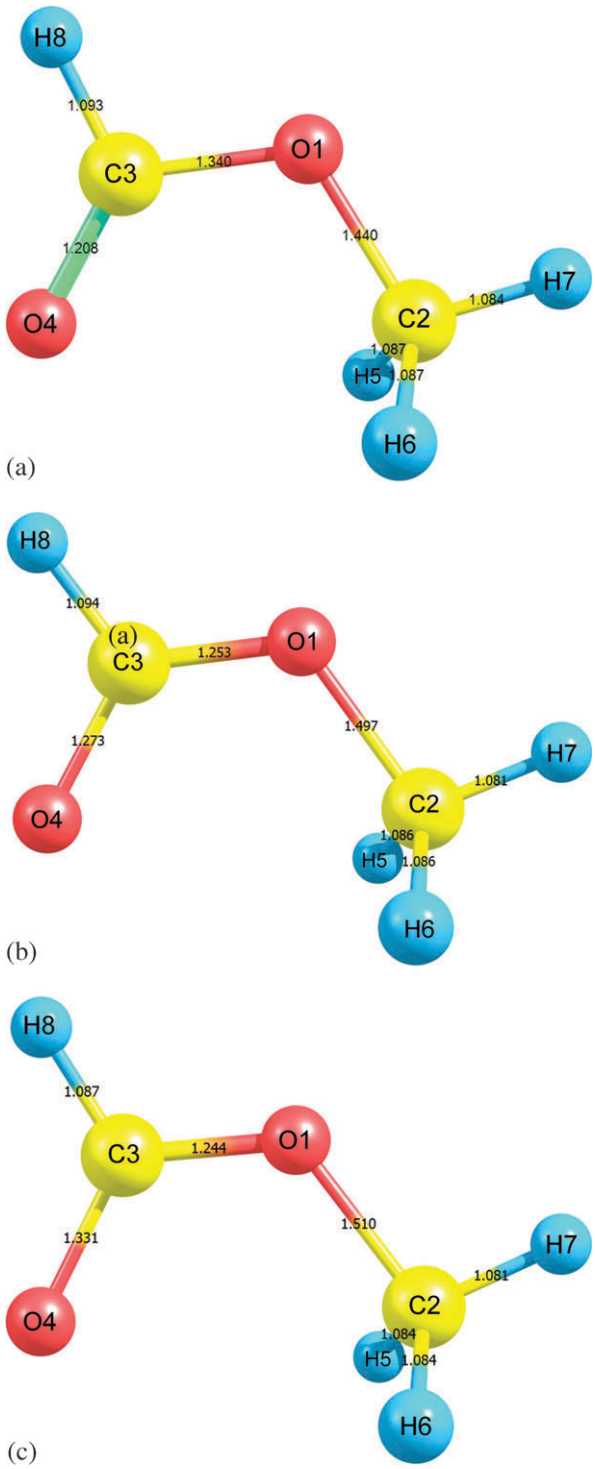

Fig. 1 Calculated structures of neutral and ionised methyl formate, $C_2H_4O_2$. (a) Neutral $\tilde{X}^1A'$, *cis*, C_s, (b) ion $^2A'$ $(3a'^{-1})$, *cis*, C_s, (c) ion $^2A''$ $(3a''^{-1})$, *cis*, C_s.

The first members of the npσ and npσ′ series are associated with the peaks at 8.492 eV ($\delta = 0.58$) and 8.682 eV ($\delta = 0.47$), respectively (Table 4). The calculated values of 8.587 and 8.940 eV (Table 1) for the two npσ series are in reasonably good agreement with the experimental values, taking into account that these transitions have valence character as well. The npσ′ series shows, for $n = 3$, vibrational excitation with two quanta of C═O stretching mode (ν_4). The feature at 9.252 eV (Fig. 5 and Table 4) is tentatively attributed to the beginning of ndσ ($n = 3$, $\delta = 0.08$) series, with calculated values of 9.204 eV (Table 1). The higher members of these Rydberg series, for which the relative intensity decreases, are difficult to assign due to the overlap with other transitions and possible vibronic structure.

The clear increase in the absorption with energy in this range (>9.5 eV) may be related to low-lying pre-dissociative or dissociative excited neutral states.

Table 5 shows some tentative assignments for features that may belong to other Rydberg series converging to the ionic electronic first excited state $\tilde{A}^2A''$ $(3a''^{-1})$. The proposed assignments for the high energy members are purely obtained on the basis of quantum defects.

5.3 Absolute photoabsorption cross-sections and atmospheric photolysis

The present optical measurements were carried out in the pressure range 0.02–1.00 Torr and reveal no evidence for changes in absolute cross-sections or peak energies as a function of pressure, thus we believe that the present spectra are free of any saturation effects. Furthermore the agreement of previous cross-sections measured at the ASTRID beamline with the most precise data available in the literature (see Eden *et al.*[34] and references therein), suggests that the present methyl formate cross-sections can be relied upon across the energy range studied up to 10.8 eV (Fig. 2).

Previous absolute VUV photoabsorption cross-sections of methyl formate are only available in the wavelength ranges 202–252 nm (6.14–4.92 eV).[4,5] Rocha *et al.* reported a cross-section at 215 nm (5.77 eV) of ~0.2 Mb,[4] which is in good agreement with the present value of 0.22 Mb.

These absolute cross-sections can be used in combination with solar actinic flux[35] measurements from the literature to estimate the photolysis rate of methyl formate in the atmosphere from an altitude close to the ground to the stratopause at 50 km. Details of the programme are presented in a previous publication by Limão-Vieira *et al.*[36] The quantum yield for dissociation following absorption is assumed to be unity. The reciprocal of the photolysis rate at a given altitude corresponds to the local photolysis lifetime. Photolysis lifetimes of less than 72 sunlit hours were calculated at altitudes above 20 km. This indicates that methyl formate molecules can be broken up quite efficiently by VUV absorption at these altitudes. At ground level the photolysis lifetimes increase to 144 sunlit hours. Recently, reactions of Cl atoms with $C_2H_4O_2$ have been studied by discharge flow-mass spectrometric methods and a coefficient rate at room temperature of $(1.01 \pm 0.15) \times 10^{-12}$ cm^3 molecule^{-1} s^{-1} was measured, meaning that these molecules may survive further from their emission sources.[37] However, methyl formate was found to be oxidised from abstraction of the carbonyl hydrogen in the presence of the hydroxyl radical,[38,39] which may provide a main reactive sink mechanism in the Earth's atmosphere. Therefore, compared with radical reactions, UV photolysis is not expected to play a significant role in the tropospheric removal of these molecules.

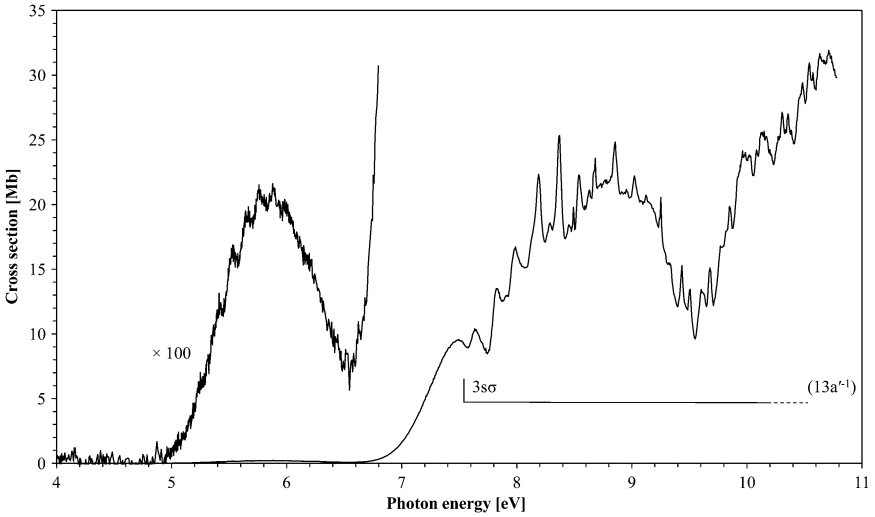

Fig. 2 VUV photoabsorption cross-section (megabarn = 10^{-18} cm^2) of methyl formate, $C_2H_4O_2$.

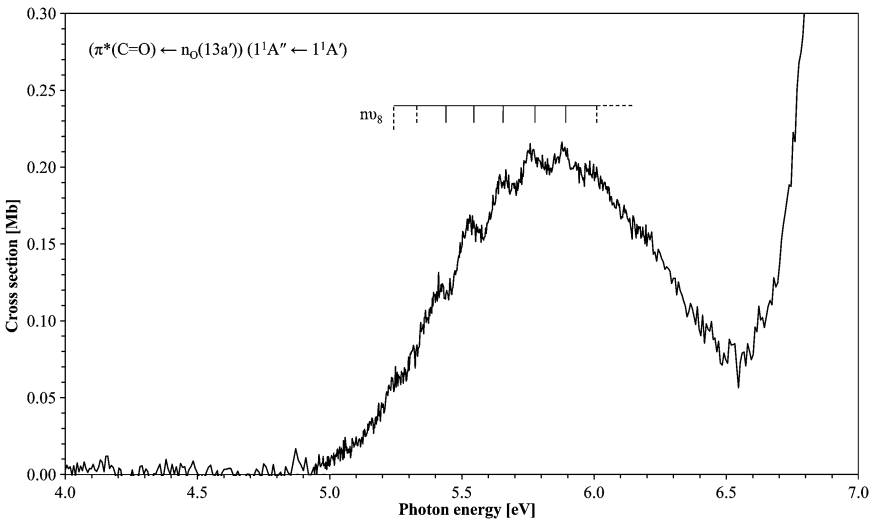

Fig. 3 Vibrational progressions in the 4.0–7.0 eV absorption band of methyl formate, $C_2H_4O_2$.

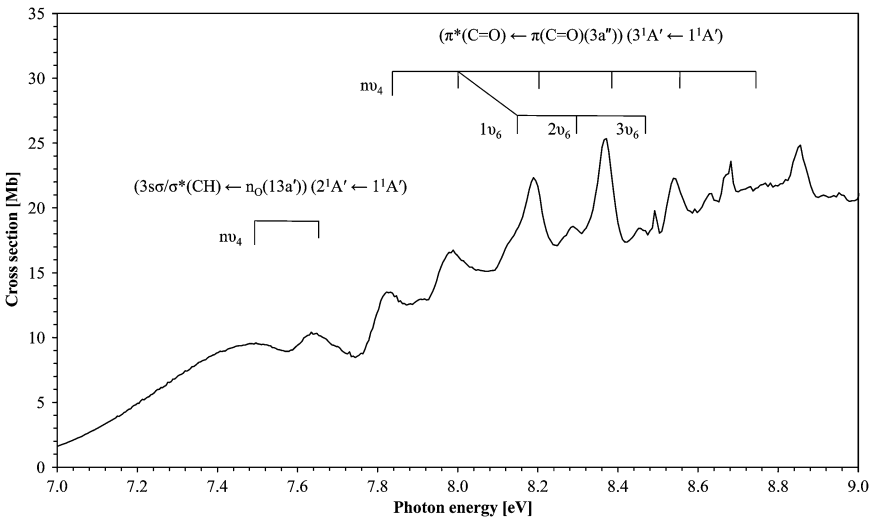

Fig. 4 Vibrational progressions in the 7.0–9.0 eV absorption band of methyl formate, $C_2H_4O_2$.

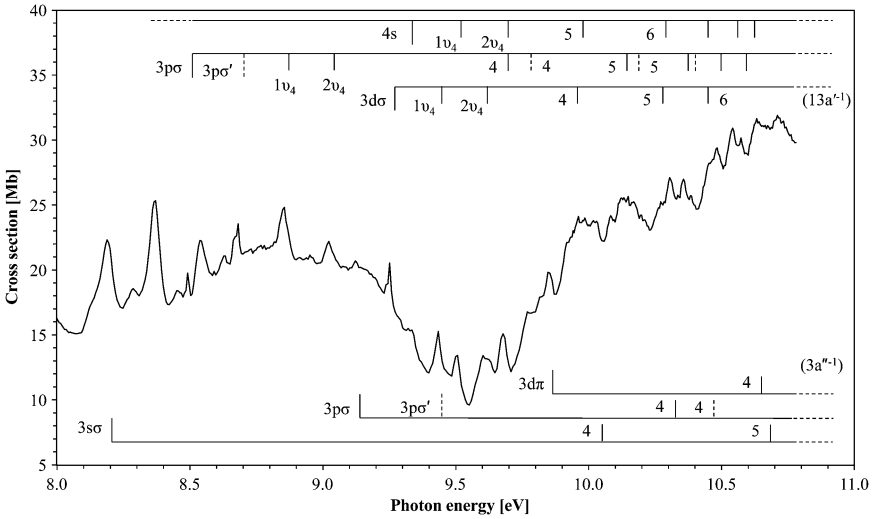

Fig. 5 Rydberg series assignment in the 8.0–11.0 eV absorption of methyl formate, $C_2H_4O_2$.

Table 3 Proposed vibrational assignments in the 5.0–6.5 eV absorption bands of methyl formate, $C_2H_4O_2$

Energy/eV	Assignment	ΔE (ν_4')/eV	ΔE (ν_6')/eV	ΔE (ν_8')/eV
First band: π*(C═O) ← n_O (13a′)				
5.22(2)	ν_{00}	—	—	—
5.31(2)	$1\nu_8$	—	—	0.09(0)
5.42(1)	$2\nu_8$	—	—	0.10(9)
5.53(0)	$3\nu_8$	—	—	0.10(9)
5.64(3)	$4\nu_8$	—	—	0.11(3)
5.75(6)	$5\nu_8$	—	—	0.11(3)
5.87(9) (v)	$6\nu_8$	—	—	0.12(3)
5.99(8)	$7\nu_8$	—	—	0.11(9)
Second band: 3sσ/σ*(CH) ← n_O (13a′)				
7.48(2) (b)	ν_{00}	—	—	—
7.635	$1\nu_4$	0.153	—	—
Third band: π*(C═O) ← π(C═O) (3a″)				
7.822	ν_{00}	—	—	—
7.989	$1\nu_4$	0.167	—	—
8.135	$1\nu_4 + 1\nu_6$	—	0.146	—
8.189	$2\nu_4$	0.200	–	—
8.288	$1\nu_4 + 2\nu_6$	—	0.153	—
8.372	$3\nu_4$	0.183	—	—
8.457	$1\nu_4 + 3\nu_6$	—	0.169	—
8.539	$4\nu_4$	0.167	—	—
8.731	$5\nu_4$	0.192	—	—

(v) means vertical value; (b) indicates a broad feature (the last decimal of the energy value is given in brackets for these less-resolved features).

6. He(I) photoelectron spectroscopy

The He(I) photoelectron spectrum of methyl formate was measured over the energy region 10.4–17.0 eV (Fig. 6). The calculated vertical IEs, using several methods, are presented in Table 2. The lowest vertical IE observed in the present PES of methyl formate (10.997 eV) agrees reasonably well with the RCCSD (11.045 eV) and RCCSD(T) (11.106 eV) theoretical predictions, the ZEKE photoelectron results of Waterstradt *et al.*[3] (adiabatic, 10.835 eV) and with Cannington and Ham[40] (adiabatic, 10.85 eV taken from ref. 41). On the other hand, the electron propagator P3 results are slightly two large. This may be surprising since that in our previous studies of several other molecules,[42–44] propagator methods (in that case ROVGF) outperformed RCCSD(T) when compared to experiment. In the case of carboxylic acids,[43] which also contain COOH groups, the agreement of ROVGF with experiment was very good.

Table 4 Energies (eV), quantum defects, and assignments of the ns, np and nd Rydberg series converging to the $\tilde{X}^2A'(13a'^{-1})$ ionic electronic ground state of methyl formate, $C_2H_4O_2$

Vertical transition energy	Quantum defect (δ)	Assignment
IE_1 = 10.812 eV[a]		
7.48(2)	0.98	3sσ
9.322	0.98	4sσ
9.500	—	$4s\sigma + 1\nu_4$
9.678	—	$4s\sigma + 2\nu_4$
9.963	0.99	5sσ
10.272	0.98	6sσ
10.43(2) (s)	1.01	7sσ
10.543	0.89	8sσ
10.60(6) (s)	0.87	9sσ
8.492	0.58	3pσ
9.679	0.54	4pσ
10.125	0.55	5pσ
10.358	0.53	6pσ
10.485	0.55	7pσ
10.574	0.44	8pσ
8.682	0.47	3pσ′
8.856	—	$3p\sigma' + 1\nu_4$
9.024	—	$3p\sigma' + 2\nu_4$
9.770	0.38	4pσ′
10.171	0.39	5pσ′
10.384	0.36	6pσ′
9.252	0.05	3dσ
9.436	—	$3d\sigma + 1\nu_4$
9.604	—	$3d\sigma + 2\nu_4$
9.943	0.04	4dσ
10.26(4) (s)	0.02	5dσ
10.43(2) (s)	0.02	6dσ

[a] Adiabatic value. (s) indicates a shoulder (the last decimal of the energy value is given in brackets for these less-resolved features).

The two MP2 (RMP2 and ZAPT) results differ noticeably from experiment, especially for the $\tilde{A}^2A''$ ($\equiv 3a''^{-1}$) where the calculated values are too large by about 1 eV. The same calculation performed using the UMP2 method implemented in Gaussian 03 gives 11.500 eV for $\tilde{X}^2A'$ ($13a'^{-1}$) and a

Table 5 Energies (eV), quantum defects, and assignments of the ns, np and nd Rydberg series converging to the $\tilde{A}^2A''(3a''^{-1})$ ionic electronic first excited state of methyl formate, $C_2H_4O_2$

Vertical transition energy	Quantum defect (δ)	Assignment
IE_1 = 11.536 eV[a]		
8.18(9) (b)	0.98	3sσ
10.031	0.99	4sσ
10.66(5) (b)	1.04	5sσ
9.123	0.62	3pσ
10.306	0.67	4pσ
9.43(6) (b)	0.46	3pσ′
10.45(4) (s)	0.46	4pσ′
9.848	0.16	3dπ
10.633	0.12	4dπ

[a] Vertical value. (b) indicates a broad feature; (s) a shoulder (the last decimal of the energy value is given in brackets for these less-resolved features).

completely unphysical value for the $3a''^{-1}$ state. This is probably connected to the large spin contamination effect (S^2 = 1.05 instead of 0.75). This failure of open shell perturbative methods has already been observed previously:[45] the use of diffuse basis functions led to a divergent behaviour of the perturbative series. Indeed, in the present case, the use of the cc-pVTZ basis set instead of the aug-cc-pVTZ gives a ZAPT ionisation energy of 12.070 eV for the $3a''^{-1}$ state instead of 12.779 eV, while the $13a'^{-1}$ does not vary. Further investigation on this topic is beyond the scope of the present study.

From the vertical calculated IE's, the resolved vibrational structure in the low energy part of the ionic ground state (Fig. 6 and 7) band corresponds without ambiguity to the $\tilde{X}^2A'$ ($13a'^{-1}$) ionic state. In order to reproduce theoretically the observed vibrations, one has to calculate the geometry of this ionic state and then obtain its harmonic vibrational frequencies. This geometry, obtained at the ZAPT level, is shown in Fig. 1(b). When compared to neutral parameters (Fig. 1(a)), one can see an increased C═O distance while the C–O is shorter on the COH side and larger on the methyl side. The calculated frequencies prove that this structure is a minimum. However, this structure is not the most stable one: the isomerisation and dissociation of methyl formate ion (presumably the $^2A'$ ($13a'^{-1}$) state) was studied previously experimentally (TPEPICO) and theoretically (G2/MP2(full/6-31G* level).[44] From Fig. 3 of ref. 46, the CH_3–O–COH^+ form is less stable than the CH_2–O–$CHOH^+$ form by 51.9 kJ mol^{-1} (0.54 eV) with a barrier of 182.4 kJ mol^{-1} (1.88 eV). This is very similar to the keto–enol isomerisation found in our recent study on carboxylic acids.[43]

Due to this rather large barrier, we may expect to see vibrations of CH_3–O–COH^+ before it has time to isomerise to CH_2–O–$CHOH^+$. So the calculated Franck–Condon factors displayed in Fig. 7(a) were obtained with the frequencies corresponding to the structure in Fig. 1(b). The theoretical peaks were convoluted by 50 meV FWHM Gaussian functions. The agreement is excellent, except for a shift between theory and experiment which increases with energy. This shift may be easily explained by the fact that the *ab initio* frequencies are a few percent too large. It is difficult to assign precisely the observed progressions, since there are many combination bands. Nevertheless, these peaks may be classified into two groups, corresponding to the observed 0.180 and 0.090 eV separations (see Table 6): the first group, corresponding to the most intense peaks separated by ~0.2 eV, is mainly due to the excitation of the ν_4 (C═O) stretching mode. The second group, beginning ~0.1 eV after the 0–0 peak, has also an energy separation of ~0.2 eV and is due to the combination between the ν_4 (C═O) and the ν_{10}(O–CH_3) stretching modes. However, other combinations, involving for example methyl vibrations, contribute to the spectrum. Similar behaviour, as far as C═O stretching mode is concerned, was observed in acetic acid,[2] from where an oxygen lone pair electron is also removed.

The high energy part of this band, centered at 11.536 eV, is assigned to the $\tilde{A}^2A(\equiv 3a''^{-1})$ state (Fig. 6 and Table 2). It has no apparent vibrational structure, suggesting that this state could be unstable. However, a geometry optimization at the ZAPT level, leads to the structure shown in Fig. 1(c). Harmonic frequency calculations prove that it is a stable minimum. The larger C═O length (1.331 Å) is consistent with the removal of

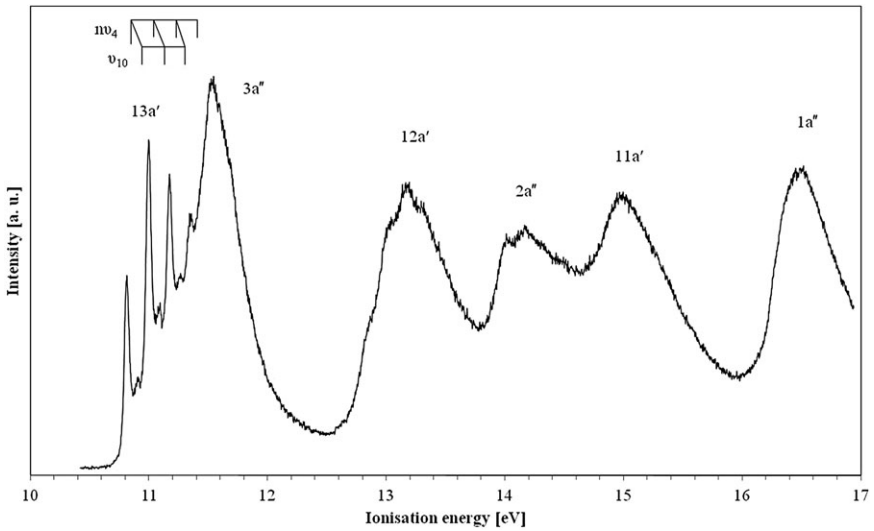

Fig. 6 He(I) photoelectron spectrum of methyl formate, $C_2H_4O_2$.

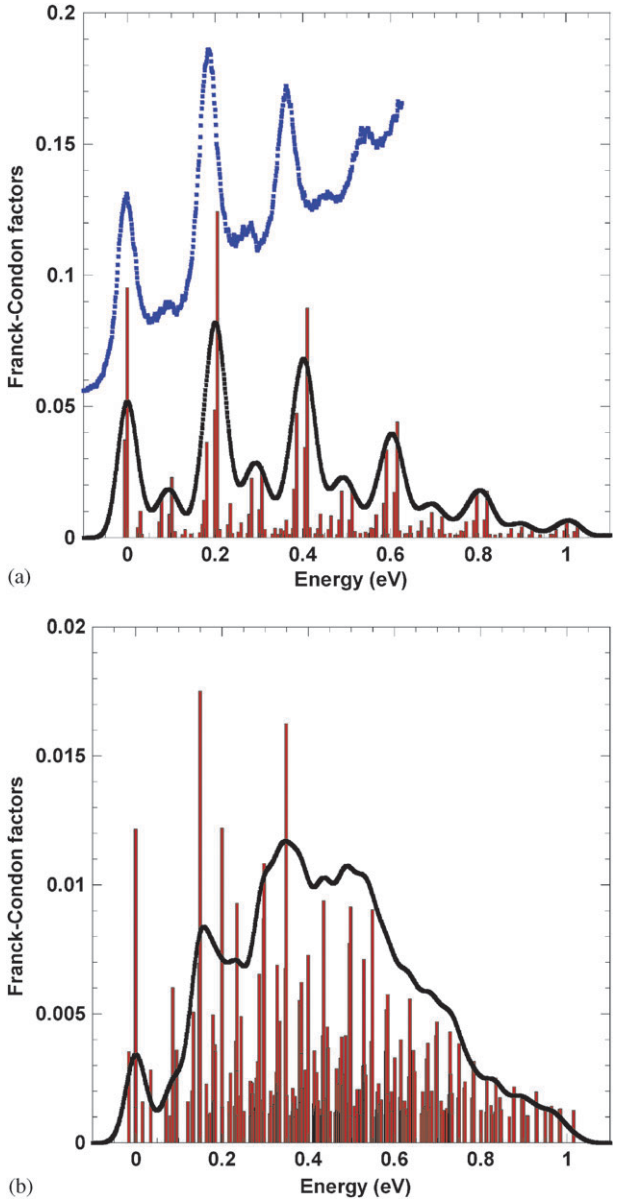

Fig. 7 Comparison between deconvoluted experimental (blue) and theoretical Franck–Condon (red and black) vibrational structures of the first photoelectron band of methyl formate. (a) Ion $^2A'$ $(13a'^{-1})$, (b) ion $^2A''$ $(3a''^{-1})$.

Table 6 Energy positions and vibrational analysis of features observed in the first photoelectron band $(13a'^{-1})$ of methyl formate $C_2H_4O_2$

Peak energy/eV	Assignment	ΔE (ν_4')/eV C=O stretching	ΔE (ν_{10}')/eV O–CH_3 stretching
10.812	Adiabatic IE	—	—
10.90(4)(b)	$1\nu_{10}$	—	0.09(2)
10.997	$1\nu_4$	0.185	—
11.08(4)(b)	$1\nu_4 + 1\nu_{10}$	—	0.08(9)
11.173	$2\nu_4$	0.176	—
11.26(1)(b)	$2\nu_4 + 1\nu_{10}$	—	0.08(8)
11.351	$3\nu_4$	0.178	—

(b) indicates a broad feature (the last decimal of the energy value is given in brackets for these less-resolved features).

the π(C=O) electron. The calculated Franck–Condon factors are shown in Fig. 7(b). These calculations prove that the apparent absence of vibration structure is due to numerous overlapping peaks. Such a behaviour is also observed in the first band of the photoelectron spectrum of NSCl.[47] The most intense progression is due to the ν_8(O–COOH) stretching at 0.205 eV (compared to 0.150 eV for neutral),[32] with combination bands involving for example ν_{10}(O–CH_3), whose value is 0.095 eV. The high energy tail of the measured spectrum is also well reproduced by the calculations. As can be seen in Fig. 7(b), the Franck–Condon factors absolute values of the two bands appear to be rather different. Unfortunately, it is not possible to combine the results of Fig. 7 to reproduce the observed spectrum because the intensity of the ionisation process for these two states cannot be calculated.

7. Conclusions

The present work provides the first complete optical electronic spectra of methyl formate and the most reliable set of absolute photoabsorption cross-sections available between 4.0 to 10.8 eV. The observed structure has been assigned to valence and Rydberg transitions on the basis of comparisons with the *ab initio* calculations of vertical excitation energies and oscillator strengths for this molecule. Fine structure has been assigned to vibrational series, dominantly involving excitation of the ν_4 (C=O) stretching mode. The high resolution He(I) photoelectron spectrum of methyl formate has enabled vibrational excitations in the ionic electronic states $\tilde{X}^2A'(13a'^{-1})$ and $\tilde{A}^2A(\equiv 3a''^{-1})$. The theoretical results are in good agreement with the experiments and predict significant mixing of Rydberg and π* states. The photolysis lifetimes of methyl formate have also been carefully derived for the Earth's troposphere and stratosphere.

Acknowledgements

PLV acknowledges the visiting fellow position in the Molecular Physics group, Open University, UK, together with M-J H-F the financial support from the Portuguese–Belgian joint collaboration. The Patrimoine of the University of Liège, the *Fonds National de la Recherche Scientifique* and the *Fonds de la Recherche Fondamentale Collective* of Belgium have supported this research. M-J H-F wishes to acknowledge the *Fonds de la Recherche Scientifique* for her position. PLV and NJM acknowledge the support from the British Council for the Portuguese–English joint collaboration. The authors wish to acknowledge the beam time at the ISA synchrotron at Aarhus University, Denmark. We also acknowledge the financial support provided by the European Commission through the Access to Research Infrastructure action of the Improving Human Potential Programme. This work forms part of the EU network Cost Action CM0601 programme ECCL. The "PhLAM" is "Unité Mixte de Recherche du CNRS". The authors are indebted to Prof. Jean-Pierre Flament for stimulating discussions.

References

1 United Nations Environment Program (UNEP), 2006 Assessment report of the Rigid and Flexible Foams Technical Options Committee, http://ozone.unep.org/teap/Reports/FTOC/ftoc_assessment_report06.pdf.
2 P. Limão-Vieira, A. Giuliani, J. Delwiche, R. Parafita, R. Mota, D. Duflot, J.-P. Flament, E. Drage, P. Cahillane, N. J. Mason, S. V. Hoffmann and M.-J. Hubin-Franskin, *Chem. Phys.*, 2006, **324**, 339.
3 E. Waterstradt, R. Jung, T. Belling and K. Müller-Dethlefs, *Ber. Bunsen-Ges. Phys. Chem.*, 1994, **98**, 176.
4 A. B. Rocha, A. S. Pimentel and C. Bielschowsky, *J. Phys. Chem. A*, 2002, **106**, 181.
5 E. Vésine and A. Mellouki, *J. Chem. Phys.*, 1997, **94**, 1634.
6 S. Eden, P. Limão-Vieira, S. V. Hoffmann and N. J. Mason, *Chem. Phys.*, 2006, **323**, 313.
7 J. Delwiche, P. Natalis, J. Momigny and J. E. Collin, *J. Electron Spectrosc. Relat. Phenom.*, 1973, **1**, 219.
8 J. H. E. Eland, *Photoelectron spectroscopy*, Butterworths, London, 2nd edn, 1984.
9 T. H. Dunning, *J. Chem. Phys.*, 1989, **90**, 1007.
10 L. Serrano-Andrés and M. Merchan, *THEOCHEM*, 2005, **729**, 99.
11 A. Dreuw and M. Head-Gordon, *Chem. Rev.*, 2005, **105**, 4009.
12 B. O. Roos, in *Theory and Applications of Computational Chemistry: The First Forty Years*, ed. C. Dykstra, *et al.*, Elsevier, 2005, ch. 27.
13 R. J. Bartlett and M. Musila, *Rev. Mod. Phys.*, 2007, **79**, 291.
14 C. Hampel, K. Peterson and H.-J. Werner, *Chem. Phys. Lett.*, 1992, **190**, 1.
15 K. Kaufmann, W. Baumeister and M. Jungen, *J. Phys. B: At., Mol. Opt. Phys.*, 1989, **22**, 2223.
16 P. J. Knowles, C. Hampel and H.-J. Werner, *J. Chem. Phys.*, 1993, **99**, 5219.
17 J. D. Watts, J. Gauss and R. J. Bartlett, *J. Chem. Phys.*, 1993, **98**, 8718.
18 H.-J. Werner, P. J. Knowles, R. Lindh, F. R. Manby, M. Schütz, P. Celani, T. Korona, A. Mitrushenkov, G. Rauhut, T. B. Adler, R. D. Amos, A. Bernhardsson, A. Berning, D. L. Cooper, M. J. O. Deegan, A. J. Dobbyn, F. Eckert, E. Goll, C. Hampel, G. Hetzer, T. Hrenar, G. Knizia, C. Köppl, Y. Liu, A. W. Lloyd, R. A. Mata, A. J. May, S. J. McNicholas, W. Meyer, M. E. Mura, A. Nicklass, P. Palmieri, K. Pflüger, R. Pitzer, M. Reiher, U. Schumann, H. Stoll, A. J. Stone, R. Tarroni, T. Thorsteinsson, M. Wang and A. Wolf, *MOLPRO, version 2009.1, a package of ab initio programs*, see http://www.molpro.net.
19 A. M. Ferreira, G. Seabra, O. Dolgounitcheva, V. G. Zakrzewski and J. V. Ortiz, *Application and Testing of Diagonal, Partial Third-Order Electron Propagator Approximation*, in *Quantum-Mechanical Prediction of Thermochemical Data*, ed. J. Cioslowski, Kluwer, Dordrecht, 2001, p. 131.
20 J. V. Ortiz, *J. Chem. Phys.*, 1996, **104**, 7599.
21 M. J. Frisch, G. W. Trucks, H. B. Schlegel, G. E. Scuseria, M. A. Robb, J. R. Cheeseman, J. A. Montgomery, Jr, T. Vreven, K. N. Kudin, J. C. Burant, J. M. Millam, S. S. Iyengar, J. Tomasi, V. Barone, B. Mennucci, M. Cossi, G. Scalmani, N. Rega, G. A. Petersson, H. Nakatsuji, M. Hada, M. Ehara, K. Toyota, R. Fukuda, J. Hasegawa, M. Ishida, T. Nakajima, Y. Honda, O. Kitao, H. Nakai, M. Klene, X. Li, J. E. Knox, H. P. Hratchian, J. B. Cross, V. Bakken, C. Adamo, J. Jaramillo, R. Gomperts, R. E. Stratmann, O. Yazyev, A. J. Austin, R. Cammi, C. Pomelli, J. W. Ochterski, P. Y. Ayala, K. Morokuma, G. A. Voth, P. Salvador, J. J. Dannenberg, V. G. Zakrzewski, S. Dapprich, A. D. Daniels, M. C. Strain, O. Farkas, K. D. Malick, A. D. Rabuck, K. Raghavachari, J. B. Foresman, J. V. Ortiz, Q. Cui, A. G. Baboul, S. Clifford, J. Cioslowski, B. B. Stefanov, G. Liu, A. Liashenko, P. Piskorz, I. Komaromi, R. L. Martin, D. J. Fox, T. Keith, M. A. Al-Laham, C. Y. Peng, A. Nanayakkara, M. Challacombe, P. M. W. Gill, B. Johnson, W. Chen, M. W. Wong, C. Gonzalez and J. A. Pople, *GAUSSIAN 03 (Revision D.01)*, Gaussian, Inc., Wallingford, CT, 2004.
22 T. D. Crawford, H. F. Schaefer III and T. J. Lee, *J. Chem. Phys.*, 1996, **105**, 1060.
23 T. J. Lee, A. P. Rendell, K. G. Dyall and D. Jayatilaka, *J. Chem. Phys.*, 1994, **100**, 7400.
24 M. W. Schmidt, K. K. Baldridge, J. A. Boatz, S. T. Elbert, M. S. Gordon, J. H. Jensen, S. Koseki, N. Matsunaga, K. A. Nguyen, S. Su, T. L. Windus, M. Dupuis and J. A. Montgomery Jr, *J. Comput. Chem.*, 1993, **14**, 1347.
25 M. S. Gordon and M. W. Schmidt, in *Theory and Applications of Computational Chemistry: The First Forty Years*, ed. C. Dykstra, *et al.*, Elsevier, 2005, ch. 41.
26 V. A. Mozhayskiy and A. I. Krylov, ezSpectrum, http://iopenshell.usc.edu/downloads.
27 L. Koziol, V. A. Mozhayskiy, B. J. Braams, J. M. Bowman and A. I. Krylov, *J. Phys. Chem. A*, 2009, **113**, 7802.
28 F. Duschinsky, *Acta Physicochim. URSS*, 1937, **7**, 551.
29 J. Demaison, L. Margulès, I. Kleiner and A. G. Császár, *J. Mol. Spectrosc.*, 2010, **259**, 70.
30 G. Cui, F. Zhang and W. Fang, *J. Chem. Phys.*, 2010, **132**, 034306.
31 M. L. Senent, M. Villa, F. J. Melendez and R. Dominguez-Gomez, *Astrophys. J.*, 2005, **627**, 567.
32 T. Shimanouchi, *Tables of Molecular Vibrational Frequencies Consolidated*, National Bureau of Standards, 1972, vol. 1, p. 107.
33 *The Role of Rydberg States in Spectroscopy and Photochemistry*, ed. C. Sandorfy, Kluwer Academic Publishers, 1999.
34 S. Eden, P. Limão-Vieira, S. V. Hoffmann and N. J. Mason, *Chem. Phys.*, 2007, **331**, 232.
35 Chemical Kinetics and Photochemical Data for Use in Stratospheric Modeling, Evaluation number 12, NASA, Jet Propulsion Laboratory, JPL Publication 97-4, January 15, 1997.
36 P. Limão-Vieira, S. Eden, P. A. Kendall, N. J. Mason and S. V. Hoffmann, *Chem. Phys. Lett.*, 2002, **364**, 535.
37 I. Bravo, A. Aranda, Y. Díaz-de-Mera, E. Moreno, M. E. Tucceri and D. Rogríguez, *Phys. Chem. Chem. Phys.*, 2009, **11**, 384.
38 D. A. Good and J. S. Francisco, *J. Phys. Chem. A*, 2000, **104**, 1171.
39 T. J. Wallington, M. D. Hurley, T. Maurer, I. Barnes, K. H. Becker, G. S. Tyndall, J. J. Orlando, A. S. Pimentel and M. Bilde, *J. Phys. Chem. A*, 2001, **105**, 5146.
40 P. H. Cannington and N. S. Ham, *J. Electron Spectrosc. Relat. Phenom.*, 1985, **36**, 203.
41 D. A. Sweigart and D. W. Turner, *J. Am. Chem. Soc.*, 1972, **94**, 5592.
42 A. Giuliani, P. Limão-Vieira, D. Duflot, A. R. Milosavljevic, B. P. Marinkovic, S. V. Hoffmann, N. Mason, J. Delwiche and M.-J. Hubin-Franskin, *Eur. Phys. J. D*, 2009, **51**, 97.
43 A. Vicente, R. Antunes, D. Almeida, I. J. A. Franco, S. V. Hoffmann, N. J. Mason, S. Eden, D. Duflot, S. Canneaux, J. Delwiche, M.-J. Hubin-Franskin and P. Limão-Vieira, *Phys. Chem. Chem. Phys.*, 2009, **11**, 5729.
44 G. Martins, A. M. Ferreira-Rodrigues, F. N. Rodrigues, G. G. B. de Sousa, N. J. Mason, S. Eden, D. Duflot, J.-P. Flament, S. V. Hoffmann, J. Delwiche, M.-J. Hubin-Franskin and P. Limão-Vieira, *Phys. Chem. Chem. Phys.*, 2009, **11**, 11219.
45 J. Olsen, O. Christiansen, H. Koch and P. Jørgensen, *J. Chem. Phys.*, 1996, **105**, 5082.
46 O. A. Mazyar and T. Baer, *J. Phys. Chem. A*, 1998, **102**, 1682.
47 D. Duflot, N. Chabert, J.-P. Flament, J.-M. Robbe, I. C. Walker, J. H. Cameron, A. Giuliani, M.-J. Hubin-Franskin and J. Delwiche, *Chem. Phys.*, 2003, **288**, 95.